JOURNAL OF MATERIALS RESEARCH AND TECHNOLOGY 2023;23:5993–6004

Available online at www.sciencedirect.com

jmr&t Journal of Materials Research and Technology

journal homepage: www.elsevier.com/locate/jmrt

Original Article

Flash sintering in metallic ceramics: finite element analysis of thermal runaway in tungsten carbide green bodies

Isacco Mazo [a,*], *Barbara Palmieri* [b], *Alfonso Martone* [b], *Michele Giordano* [b], *Vincenzo M. Sglavo* [a,c]

[a] *University of Trento, Department of Industrial Engineering, Via Sommarive 9, 38123 Trento, Italy*

[b] *Institute for Polymers, Composites and Biomaterials, National Research Council of Italy, P.le E. Fermi 1, 80055 Portici (NA), Italy*

[c] *INSTM, National Interuniversity Consortium of Materials Science and Technology, Via G. Giusti 9, 50121 Firenze, Italy*

ARTICLE INFO

Article history:
Received 9 January 2023
Accepted 26 February 2023
Available online 2 March 2023

Keywords:
Flash sintering
Thermal runaway
Finite element methods
Tungsten carbide

ABSTRACT

Flash sintering is a powerful tool for the ultrarapid consolidation of green ceramic compacts, although its activation mechanisms in electrically conductive PTC (Positive Temperature Coefficient for resistivity) materials' is poorly understood. It was argued that a flash event could be initiated and sustained for a transitory period in certain PTC ceramics because of an initial negative dependence of the green material resistivity with temperature. The thermal runaway phenomenon and its activation conditions on binderless tungsten carbide (WC) green bodies are investigated in the present work by numerical simulations using finite element methods (FEM). The flash event is recreated and studied within the COMSOL Multiphysics software at the macroscale, i.e., considering the flash as an electrical power surge driven by an increasing sample's conductivity. During the flash, very high temperatures in the range of 1800–2000 °C can be reached in the WC green sample in a few seconds. The accurate numerical simulation of such event results in heating rates exceeding 1000 °C/s, a condition that theoretically brings a powder compact at temperatures high enough to accelerate and prioritize sintering densifying mechanisms over non-densifying ones. Therefore, the sample's regions where the maximum sintering temperature is reached more slowly because of thermal contacts with the electrodes remain highly porous at the end of the process.

* Corresponding author.
E-mail address: isacco.mazo@unitn.it (I. Mazo).

https://doi.org/10.1016/j.jmrt.2023.02.213

1. Introduction

Flash sintering (FS) allows a remarkable reduction of temperature and especially the time required to consolidate a vast group of ceramic materials. When a green sample is exposed to the right combination of electric field and furnace temperature, an ultrafast diffusion phenomenon allows densification to take place in few seconds. This very quick nature is connected to the abrupt increase of conductivity in the green ceramic body internally subjected to intense Joule heating. For this reason, the flash sintering phenomenon has been primarily attributed to the thermal runaway of the ceramic's electric resistivity [1]. Theoretically, this condition hinders the applicability of said technology to materials, like metals, which possess a positive temperature coefficient (PTC) for resistivity or, in other words, when the electrical conductivity decreases with temperature. In addition, conductivity variation with temperature in PTC materials is also weak to allow a burst in the electrical power dissipation and consequently induce a flash event [2].

Very few works reported the effects of an electric current applied to PTC green samples, in a "flash sintering" configuration to allow the current to interact exclusively with the powdered material. Lagos et al. [3] and Montes et al. [4] implemented an electric-current assisted sintering (ECAS) process on metals (Fe) and hard-metals (WC–Co), forcing very high currents (4–10 kA) through the green materials. Mei et al. [5] sintered a silver paste under a high direct current of 6 kA by similar ECAS process. Very high current densities applied to low melting point materials favour a liquid phase which greatly boosts the diffusion during sintering. These previous works showed remarkable short-term sintering (1–2 s) but did not discuss any relation between accelerated sintering and the evolution of the material resistivity. In a more conventional FS experiment, Al particles were partially consolidated at high electric fields (175–330 V/cm), during a transition of the material conductivity, probably due to the presence of an oxide (Al_2O_3) film [6].

Only recently, pure WC powders were demonstrated to densify in a few seconds by using ECAS/FS route, the green sample being placed under a limited pressure between two electrodes [7,8]. A similar flash sintering set-up was implemented to consolidate yttria-stabilized zirconia cylindrical samples [9]. In WC, a transition in the material conductivity was registered under the application of low voltages (3–4 V) and moderate currents (1000–2000 A), this generating exceptional heating and sintering rates. The absence of any liquid phase in pure WC, the burst in the dissipated electrical power and its ultrafast densification demonstrate how a thermal runaway can be responsible for the accelerated sintering in a PTC material [7]. It was argued that such a phenomenon is related to the dependence of the green material's resistivity on temperature, it being negative (NTC) rather than positive (PTC) up to a certain temperature.

The present work aims at studying by numerical simulation using finite element methods (FEM) the relationship between the material electrical properties and the possibility of activating a thermal runaway phenomenon in WC green bodies. An electrical-thermal simulation is carried out to analyse the temperature evolution during the current application and the physical conditions, if any, for the thermal runaway/flash onset in a material (WC) with metallic-like electrical behaviour. The simulation results are then compared and verified with the experimental results obtained from flash sintering tests carried out using WC nanopowders.

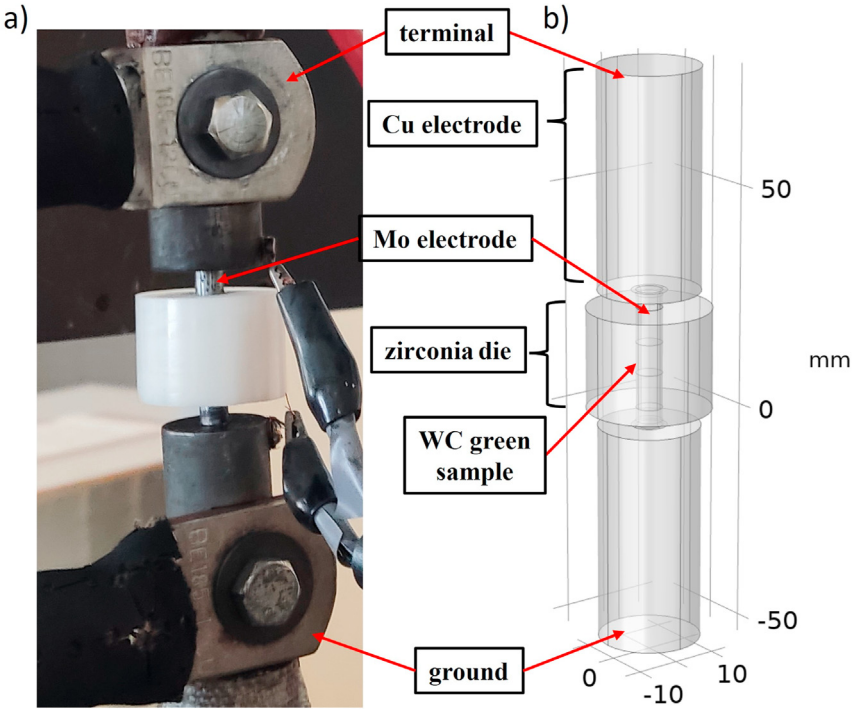

Fig. 1 – Sintering apparatus for ERFS experiments (a) and its 3D CAD model (b).

2. Materials & methods

The sintering apparatus implemented for the electrical resistance flash sintering (ERFS) experiments (Fig. 1, a) was modelled into a 3D object by CAD software (Fig. 1, b) and imported into the simulation environment of COMSOL Multiphysics ver. 5.6. The (ERFS) apparatus consists of two cylindrical molybdenum electrodes placed in contact with the green sample within an insulating cylindrical zirconia die. The molybdenum elements are connected to an external power supply (TECNA® Item 3484) through thick copper electrodes. The entire system is mounted on a mechanical testing machine which serves as a servo-hydraulic actuator, thus allowing control of the axial displacement of the two electrodes in contact with the sample under a given pressure. A typical sintering cycle consists of four steps: (i) insertion of the green ceramic sample (disk or cylinder) inside the zirconia die, (ii) placement of the electrodes in contact with the specimen at a specific pressure, (iii) application of the electric current to the sample through the electrodes to induce sintering and (iv) cooling and extraction of the sample from the die. The flash sintering procedure starts when the two electrodes are in contact with the sample and the current is turned on and typically finishes 10 s after the current application. The entire process takes place in the air. More details can be found in previous work [7].

In the present work, the flash sintering of pure WC nanopowders was modelled at the macroscopic scale [10] by coupling the equations governing the heat generated by the electric current with those of the heat transfer in solids. Three types of heat losses were considered: (i) conductive heat flux through materials adjacent to the WC sample (zirconia die and molybdenum/copper electrodes), (ii) convective heat flux between the hot surfaces and surrounding air with a heat transfer coefficient h = 5 W/(m^{2}K) and (iii) radiative heat flux with the emissivities reported in Table 1. The simulated heat source consists of the Joule heating developed by an electric current flowing through the electrodes and the WC pellet between the terminal and the ground, the initial voltage and the maximum current being the two fundamental variables. The current was controlled by COMSOL with the AC/DC module, which set the electrical boundary conditions to apply either a current or a voltage to the sample. The simulation of a flash event requires modelling the behaviour of a power supply which must switch dynamically from voltage to current-controlled power output during the abrupt increase of the sample conductivity [11,12]. In the COMSOL environment, this dynamical switch could be implemented through the "Events interface" module [13], which can model a power source driving a system that exhibits variable resistance. A real power supply can provide a constant current up to some peak voltage or a constant voltage up to some peak current. Therefore, the Events interface operated a switch between constant-voltage to constant-current mode when either the maximum voltage or current (I_lim) was reached. The experiment was initially subjected to voltage control, i.e., a certain voltage (V_app) was applied. Then, as the sample's conductivity increased, a limiting current (I_lim) was selected to prevent the uncontrolled generation of heat (Fig. 2).

The FEM simulation was performed on the 3D CAD model shown in Fig. 1 (b) using the material properties reported in Table 1. Here, only the values at room temperature are reported for simplicity and the cited references were considered for the temperature dependence function. Only the emissivity was considered invariant with temperature. The zirconia die was considered an electrical insulator, being the electric field used in the experiments too low to induce a significative Joule heating in the material [1,2,11]. The mesh was built by the COMSOL software using the physics-controlled built-in module, selecting a "Fine-mesh" setting (Fig. 6 (a)). The physical problem was solved in the time-dependent domain, from 0 to

Table 1 – Materials parameters used in the simulation.

Material	Properties	Value at 20 °C	Reference
Copper (Cu)	Emissivity	0.3	[14]
	Electrical resistivity	1.6E^{-8} (Ωm)[a]	[15], *
	Thermal conductivity	400 (W/mK)[a]	[16], *
	Heat capacity	388 (J/kgK)[a]	[16], *
	Density	8700 (kg/m^3)	*
Molybdenum (Mo)	Emissivity	0.1	[17]
	Electrical resistivity	3.8E^{-8} (Ωm)[a]	[15]
	Thermal conductivity	140 (W/mK)[a]	[16], *
	Heat capacity[†]	220 (J/kgK)[a]	[16], *
	Density	10200 (kg/m^3)	*
Zirconia	Emissivity	0.95	[14]
	Electrical resistivity	/[b]	
	Thermal conductivity	2.5 (W/mK)[a]	[16], *
	Heat capacity	450 (J/kgK)[a]	[16], *
	Density	6050 (kg/m^3)	*
Tungsten carbide (green)	Electrical resistivity	1E^{-3} (Ωm)[a]	[7]
	Thermal conductivity	110 (W/mK)[a]	[18,19]
	Heat capacity	180 (J/kgK)[a]	[18,19]
	Density	6252 (kg/m^3)	[7]

[a] The temperature dependence function is reported in the cited references; * COMSOL 5.6 Materials library.
[b] Zirconia is considered an insulator.

10 s, and the simulated results were stored with an integration time step of 0.1 s.

The microstructure of a real WC sample consolidated by the ERFS process at 3.7 V and under a maximum current of 1000 A was investigated by FESEM analysis (ZEISS® Supra40). Cross-sectional images were obtained by cutting a flash-sintered WC sample in the direction of the applied current and after subsequent grinding and polishing sequences with diamond pastes down to 1 μm. Different FESEM images were acquired on the cross-section and the microstructure was compared with the temperature gradient as evaluated from the simulation results.

3. Results & discussion

3.1. Simulation of the flash event

Previous flash sintering experiments on WC green pellets under 3.7–4 V initial voltage and 1000 A limiting current showed almost complete densification of the material [7,8]. Such electrical parameters, together with the evolution of the material resistivity (Fig. 3) as a function of temperature, were used as the starting point for the FEM simulation. Fig. 4 shows the different attempts to simulate the flash event for increasing initial voltage (V_app) from 3 V to 7 V.

The application of an increasing voltage results in an evolution of the material's temperature only between 6.3 V and 7 V (Fig. 4, a). For example, under 6.5 V the sample temperature increases slowly for 6 s and then it abruptly reaches about 1600–1700 °C (Fig. 4, a). Heating occurs at an exceptional rate (around 1000 °C/s) and corresponds to a drop in the material resistivity by several orders of magnitude (Fig. 4, b). To better understand the nature of the phenomenon generating this ultrafast heating, the energy balance between the heat generated by Joule heating (Fig. 6, b) and the heat lost from the WC sample by conduction, convection and radiation (Fig. 6, c) is reported in Fig. 5. The corresponding values (W_{in} and W_{out}, respectively) are integrated over the specimen's volume and surface domains.

The heat generated by Joule heating, W_{in}, depends almost exclusively on the interaction of the electric current with the specimen (Fig. 6, b) since the green body resistivity (Fig. 3) is orders of magnitude larger than that of the electrodes (Table 1). The heat losses, W_{out}, are instead dominated by the direct contact of the electrodes with the sample (Fig. 6, c). The zirconia die strongly limits the lateral heat losses, resulting in a large temperature gradient across the ceramic die (Fig. 5, c). When the current is supplied to the system, the sample starts to heat up at a limited rate, in a regime where $W_{out} > W_{in}$ (Fig. 5, a), i.e., the heat losses from the sample are larger than the power generated by Joule heating. This contributes to increase the temperature in the zirconia die and the molybdenum electrodes. This situation evolves slowly for about 6 s while the sample temperature gradually increases up to about 300 °C where there is the inversion between the two power curves ($W_{out} < W_{in}$). Such temperature (≈300 °C) corresponds more or less to the value at which the WC green resistivity starts to decrease (Fig. 3), thus creating the condition for a thermal runaway of Joule heating. During said event, the heat

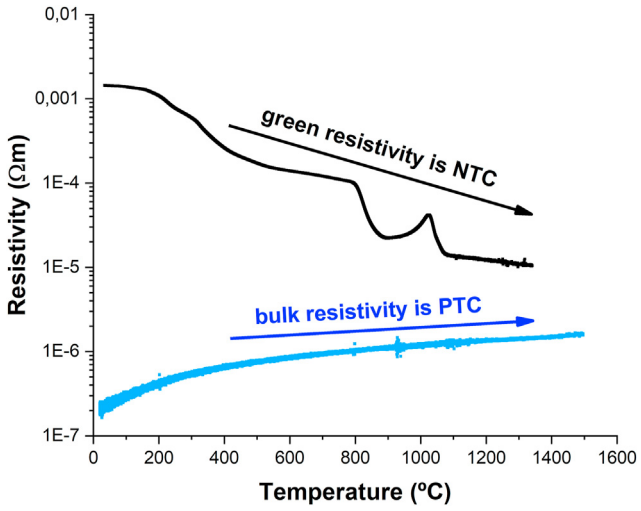

Fig. 3 – Dependence of the WC electrical resistivity on temperature. Results are reported from [7] for the material in the green and bulk states.

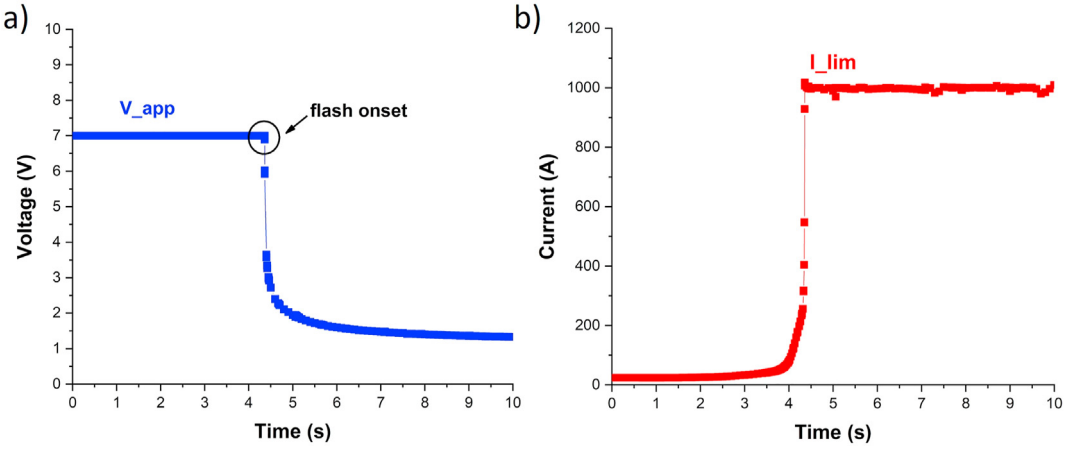

Fig. 2 – Example of transition from voltage (a) to current (b) controlled sintering regime by using the COMSOL Events interface (simulation results at 7 V).

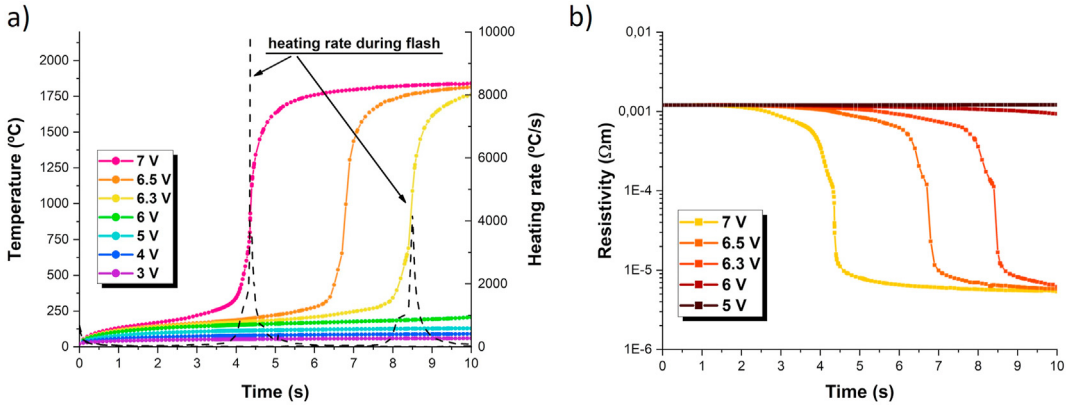

Fig. 4 – Simulation results of the average temperature and heating rate in the WC pellet under different applied voltage (a) and corresponding material's resistivity evolution (b) as a function of time.

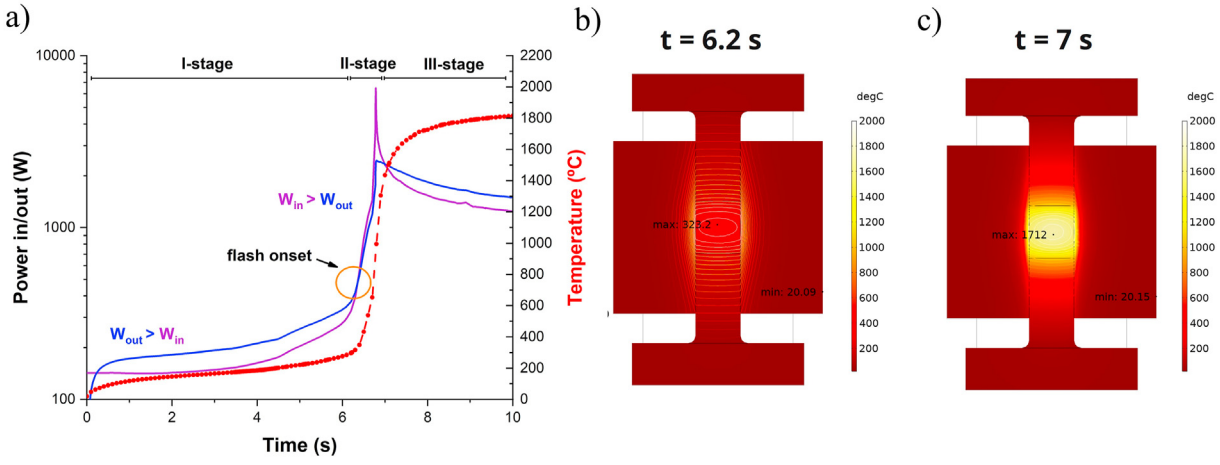

Fig. 5 – Balance between the power generated by Joule heating, W_{in}, and the dissipated one, W_{out}. Temperature distribution within the zirconia die before (b) and after the onset of the flash event (c).

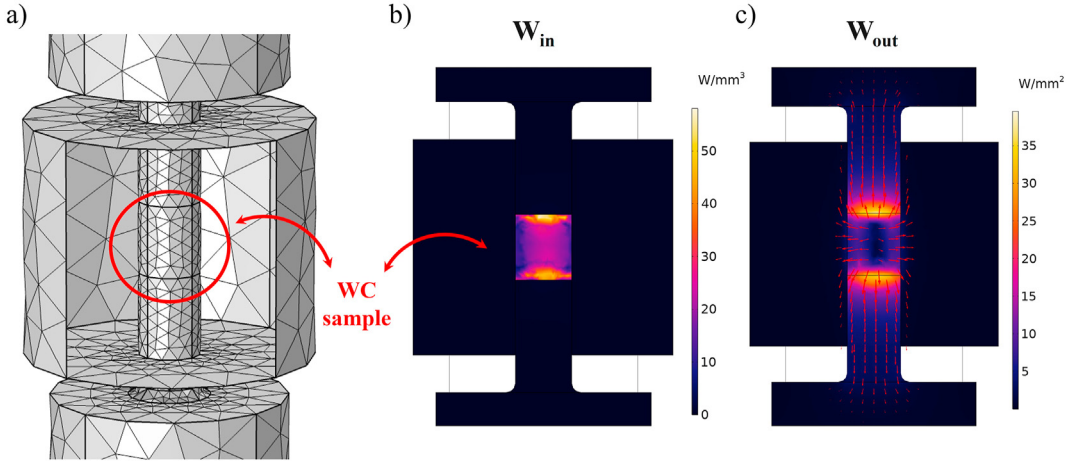

Fig. 6 – Detail of the mesh within the zirconia insulating die (a) and its cross sections (b, c) showing the simulation results at 6.5 V during the flash event (t = 6.8 s). W_{in} = heat generated in the WC sample by Joule heating (b); W_{out} = heat losses (conduction, convection and radiation) (c).

generated within the sample largely increases because of the higher conductivity (Fig. 5, a), up to the point where it cannot be dissipated quickly enough through the electrodes [20]. The condition for the flash onset can be correctly addressed to the intersection of W_{out} and W_{in} curves after 6 s simulation time. In this time frame, the sample temperature increases at a huge rate with respect to the system as shown in Fig. 5 (b and c). The temperature continues to increase very quickly up to 1600 °C when the conductivity of the sample is so high to allow the maximum current of 1000 A to flow through the material (Fig. 2, b).

At around 9 s and with a sample temperature above 1800 °C, the resistivity reaches a value around $4x10^{-6}$ Ω m (Fig. 4, b), very close to that of bulk tungsten carbide at high temperatures (Fig. 3). At this condition, the material resistivity no longer possesses a NTC characteristic and the thermal runaway/flash event spontaneously terminates.

The end of the runaway event at the maximum allowed current of 1000 A slows down the heating process; the system is again characterized by the inversion between W_{out} and W_{in} curves and this results in a slow increase of temperature above 1600 °C. It is worth pointing out the strong similarity between the present flash sintering experiment and those more traditionally performed on free-standing ceramic powder green compacts [21,22]. Even if this flash sintering set-up operates in open-air conditions and at room temperature, the typical three stages of flash sintering can be identified in Fig. 5 (a). During stage I (incubation time) the sample temperature increases slowly due to the limited amount of Joule heating; in stage II (flash onset) an abrupt escalation of the material conductivity occurs, and it allows a surge in the dissipated electric power; during stage III (constant current regime) the maximum current limit is reached and the sintering continues with a moderate temperature increase.

Flash sintering of WC green samples is achievable in a specific sintering set-up, where the heat losses from the ceramic sample are partially limited due to a combination of material properties and high current density supply. The conductive nature of tungsten carbide requires a huge amount of current to sustain the flash phenomenon and to reach the high temperature necessary to sinter the material. As shown in Fig. 5 (a), the activation of the flash sintering phenomenon on tungsten carbide opens the possibility of reaching very high temperatures (1700-1800 °C) with an incredibly fast heating rate (10^3 °C/s), thus resulting in an ultrafast consolidation of the starting powders [7,8]. The applicability of FS to conductive refractory materials and ultra-high temperature ceramics (UHTC) can offer a valid alternative to more complex FAST/SPS processes, which require complex equipment and far more processing energy [23].

The activation of a thermal runaway event was therefore successfully simulated for a conductive ceramic, although a significantly higher voltage (6.3 V) was shown to be required to activate the flash event with respect to the experimental evidence (3.7 V) (Fig. 8). This discrepancy will be analysed in detail in the following section, introducing the concept that a powder compact does not behave like a homogeneous material when it is crossed by an electric current. Heat is not generated homogeneously, as simulated by FEM, but it is localised in the region of higher resistance, like particle–particle contacts [10,24].

3.2. *Two-dimensional disks concept for modelling the particle surface overheating*

As shown in Fig. 8 and also reported in the temperature evolution plot in Fig. 4 (a), the simulated flash event requires a higher initial voltage (6.3 V) to be triggered with respect to the experimental data (3.7 V). The green sample is composed of particles with an average size of about 240 nm, their direct simulation by FEM analysis being almost technically impossible, considering that the specimen contains millions of single elements. Alternatively, the local interaction of the electric current at the particle–particle contacts can be represented by analysing the electrical effect generated at such contact points (Fig. 7, d). The particle–particle contacts are characterized by the nanometric size and the surface chemistry of WC nanoparticles. To simplify the problem, a 2D disk

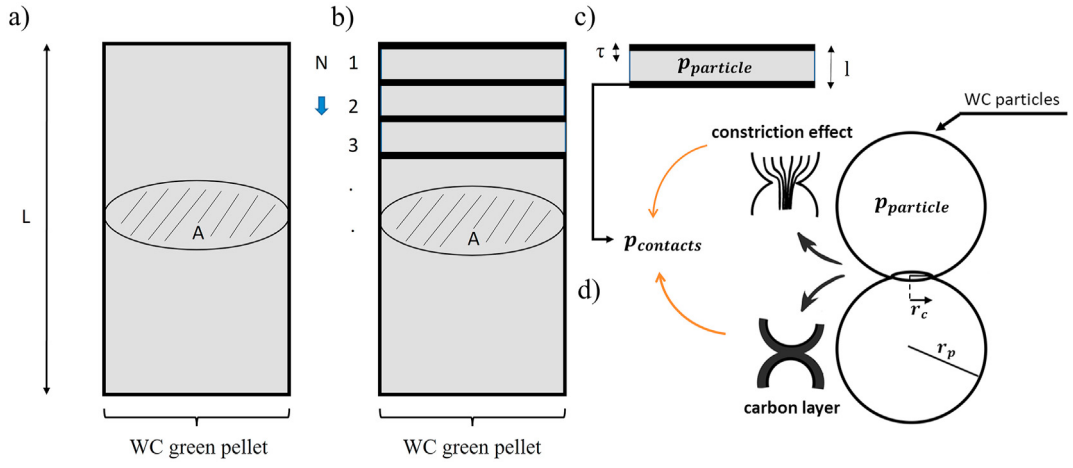

Fig. 7 – Schematics of the 2D model used for studying the overheating in the WC sample: pellet with homogeneous electrical properties (a) and pellet sectioned in disks with resistive interfaces (b). Every disk is characterized by two regions with low and high resistivity (c) where the former represents the internal resistivity of WC nanoparticles ($\rho_{particle}$) and the latter characterizes the higher resistivity at the contact points ($\rho_{contacts}$) (d).

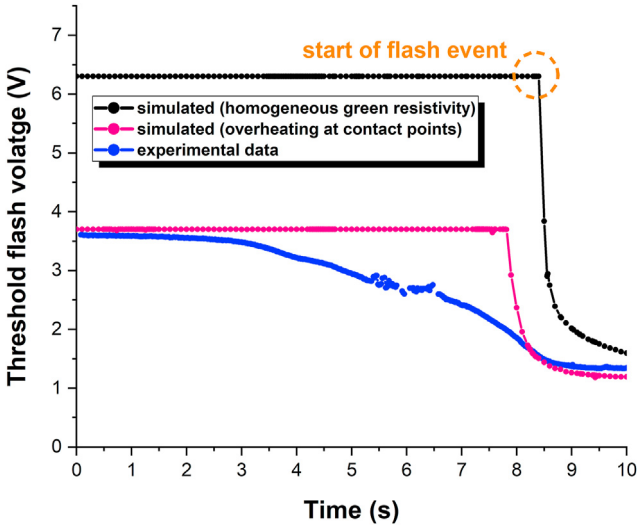

Fig. 8 – Comparison between experimental and simulation results: threshold flash voltage required for triggering the runaway phenomenon.

model can be developed to study the overheating occurring at the interfaces between the WC particles (Fig. 7). The model considers a green pellet consisting of N number of cylindrical disks, where each disk is composed of two regions: an internal one, representing the resistivity developed within a WC particle ($\rho_{particle}$) and an outer one characterized by the increased resistivity at the contacts points ($\rho_{contacts}$).

Every disk contains two layers of higher resistance where the heat is localised upon the current flow. The thickness of these layers (τ) and their resistivity are evaluated in such a way as to simulate the real effect of the localisation of the current between nanometric particles. The effect of heat localisation on the flash onset conditions requires that the average electrical power dissipation (P_{avg}) between the two pellets of Fig. 7 (a) and (b) are identical. Therefore:

$$P_{avg}^{hom} = P_{avg}^{disk} \tag{1}$$

where:

$$P_{avg}^{hom} = RI^2 = \rho_{exp}\frac{L}{A}I^2 \tag{2}$$

is the average power dissipation for the homogenous pellet (Fig. 7, a) and

$$P_{avg}^{disk} = \sum \rho_{particles}\frac{(l-2\tau)I^2}{A} + \sum \rho_{contacts}\frac{\tau}{A}I^2 \tag{3}$$

is the average power dissipation for the pellet sectioned in N disk (Fig. 7, b), ρ_{exp} being the experimental resistivity of a green pellet (Fig. 3), L the height of the pellet, A the cross-section area of the pellet, l the height of the single disk and τ the thickness of the layer (Fig. 7, c). If one considers that $N = \frac{L}{l}$, Eq. (1) becomes:

$$\rho_{exp} = \frac{N}{L}\left(\rho_{particle}(l-2\tau) + \rho_{contacts}\tau\right) \tag{4}$$

which, by simple rearrangement, yields:

$$\tau = \frac{L}{2N}\frac{\left(\rho_{particle} - \rho_{exp}\right)}{\left(\rho_{particle} - \rho_{contacts}\right)} \tag{5}$$

The particles ($\rho_{particle}$) and the contacts ($\rho_{contacts}$) resistivity can be evaluated according to the theory of small electrical contacts [25], and to the model developed by [26] for the contacts size effect on the flash sintering of ionic nanoparticles. In addition, WC nanoparticles are natively covered by a carbon nanolayer which influences the electrical contacts and, consequently, the overall resistivity of the green pellet [27]. The overall resistivity of a WC green pellet (ρ_{exp}) can be related to the bulk resistivity of tungsten carbide (ρ_{bulk}) and the resistivity of surface carbon (ρ_{carbon}) according to the following equation:

$$\rho_{exp} = \rho_{tot.pellet} = \frac{4}{9}\pi\frac{r_{particle}}{r_{contact}}\left(\frac{\rho_{bulk}}{\pi} + \frac{\rho_{bulk}}{4} + \frac{2\rho_{carbon}thickness}{\pi r_{contact}}\right) \tag{6}$$

where thickness is referred to the depth of the surface carbon layer previously reported in [27].

The overall resistivity of a granular pellet can be split into two parts: (i) the internal contribution of the particles ($\rho_{particles}$):

$$\rho_{particle} = \frac{4}{9}\pi\frac{r_{particle}}{r_{contact}}\left(\frac{\rho_{bulk}}{\pi}\right) \tag{7}$$

and (ii) the contributions of the constriction resistance and that of the surface carbon layer ($\rho_{contact}$):

$$\rho_{contact} = \frac{4}{9}\pi\frac{r_{particle}}{r_{contact}}\left(\frac{\rho_{bulk}}{4} + \frac{2\rho_{carbon}thickness}{\pi r_{contact}}\right) \tag{8}$$

After the evaluation of $\rho_{particles}$ and $\rho_{contact}$, the simulation can be solved according to Eq. (5) for a WC pellet consisting of an arbitrary number of disks (N), N being the input parameter, for an output represented by a specific value of τ. The thickness of the layer (τ), which represents the modification of the local electrical properties at the contact points ($\rho_{contact}$), requires that the average resistivity of the two pellets (Fig. 7 (a) and (b)) is the same, because of the imposed condition, $P_{avg}^{hom} = P_{avg}^{disk}$. This means that, by average, the same Joule heating occurs in the two pellets during the flash phenomenon, although in the model composed of N disks more heat is generated at the contact points between the disks with respect to the internal part. This is the same as having a non-homogeneous temperature distribution, in the form of a local overheating during the flash event, thus better representing the real phenomenon occurring between two particles in contact. The accuracy of such model can be refined indefinitely by increasing the parameter N, resulting in a layer thickness (τ) as small as required. Potentially, with adequate computational power, N can be set high enough to reach an interface thickness (τ) similar to the interaction length among the real nanoparticles.

3.3. *Effect of heat localisation on the flash onset conditions*

The simulation results with N equal to 10 (Fig. 9, b) show how the 2D disk model successfully simulates a flash event at the

same voltage recorded experimentally (Fig. 8). The flash event can be triggered at 3.7 V (Fig. 8) in the pellet that models the localisation of Joule heating at the interfaces. This means that the pellet with an increased interface resistivity allows to reach, locally, temperatures high enough to have a drop in the material resistivity and to initiate a thermal runaway phenomenon at lower applied voltages. This can also be proven by the temperature evolution plotted in Fig. 9 (a) for the two pellets of Fig. 9 (b) and (c). The average temperature of the two pellets remains almost the same along the process, the difference regarding the flash event starting time. This is connected to the effect of the initial voltage on the flash onset time, because a higher initial value shortens the heating incubation time (Fig. 4, a).

Fig. 9 shows the important contributions of the overheating at the particle–particle contacts on the flash phenomenon. The rapid temperature increase at the higher resistance regions contributes to lowering the voltage and so the electrical power consumption for starting the runaway event. This is remarkable since the application of a lower overall electrical power allows a very similar temperature evolution in the material during the test (Fig. 9, a).

As a proof of concept, the use of the 2D disk model (Fig. 7, b) for simulating the particle overheating effect was validated for

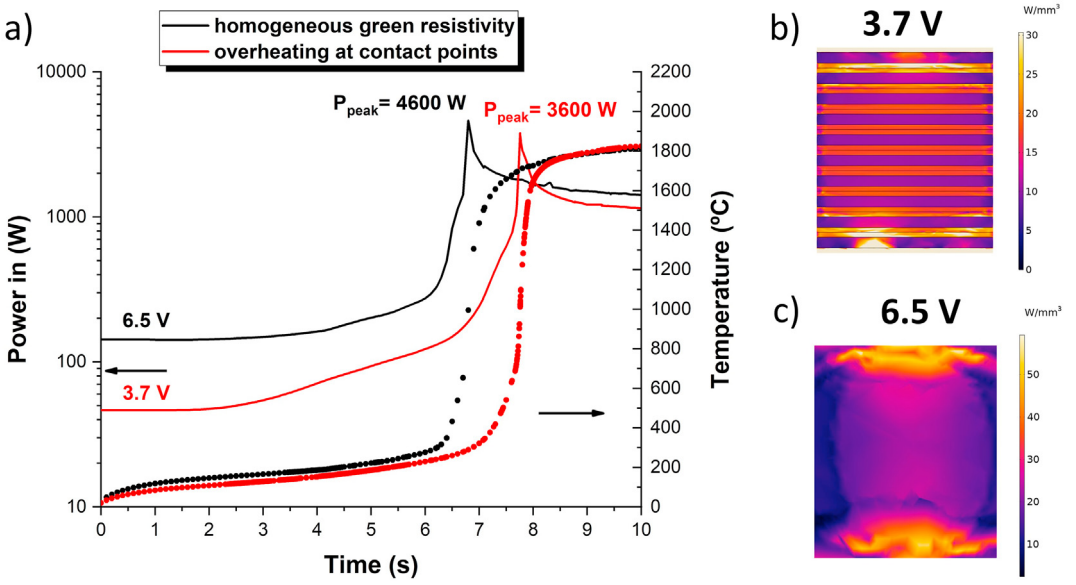

Fig. 9 – Simulation results of the dissipated electrical power and temperature generated during the flash experiments: (a) Joule heating generated in the WC sample in the case of the 2D disk model (N = 10) and (b) for a pellet with homogeneous resistivity (c).

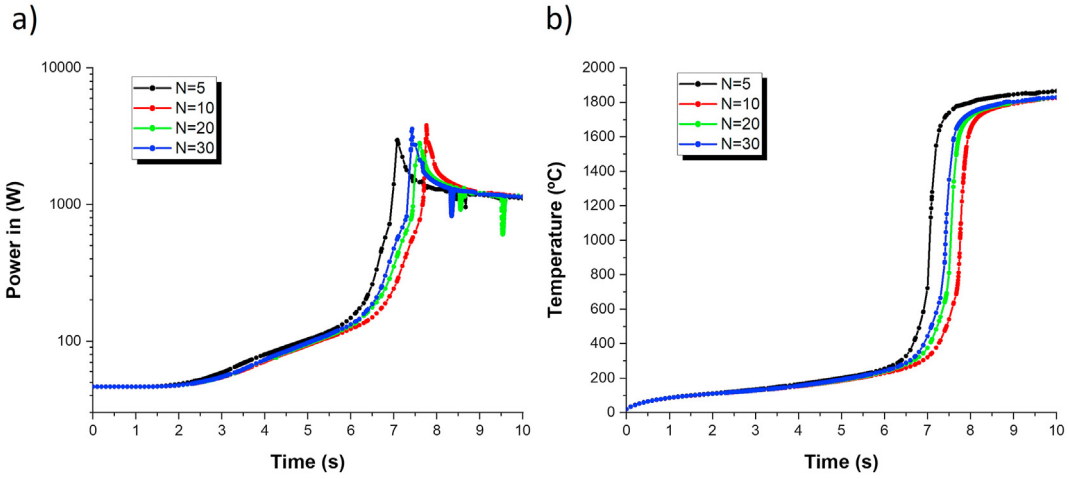

Fig. 10 – Simulation results showing the electrical power dissipation (a) and the corresponding temperature generated (b) by simulating the particle overheating with different N values.

different N values. Fig. 10 shows the results for the power consumption and temperature generated in the WC green pellet for different N values. It is possible to verify how, by increasing the number of disks (N), similar results can be obtained without the appearance of any trend, the position of the power peak (Fig. 10, a) not changing with N. This result is in line with the concept of the 2D disk model, where the layer thickness (τ), depending on the parameter N, imposes the equality in the average pellet resistivity, hence in the average dissipated electrical power (Eq. (3)) (Fig. 10, a).

3.4. *Temperature distribution effect on WC sample densification*

Fig. 6 (b) and (c), which show the heat generated and lost in the WC samples, point out intense heat exchange, during the

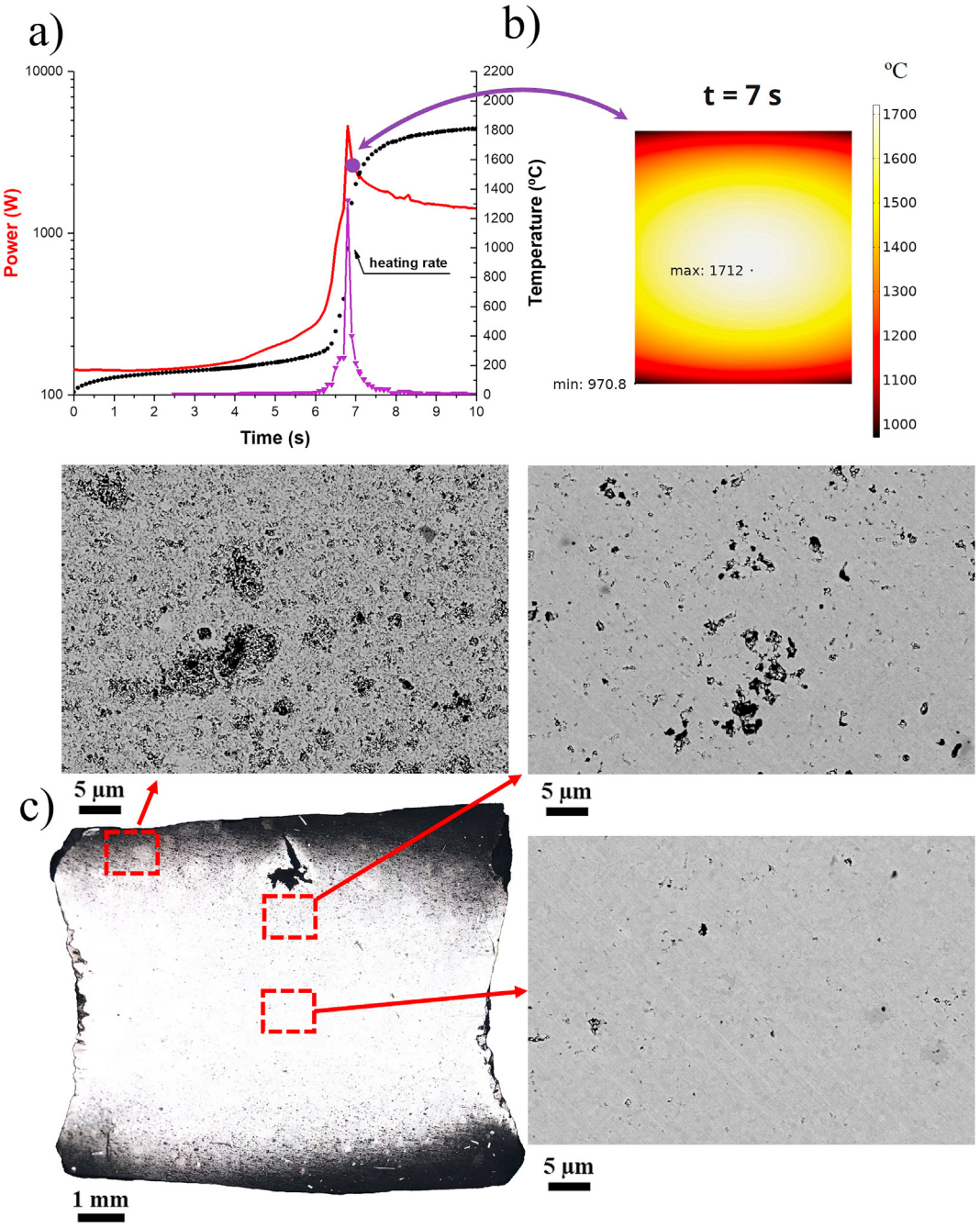

Fig. 11 – Simulated evolution of dissipated power, temperature and heating rate during flash sintering, measured in the WC sample. The temperature map (b) is shown for a cross-section of a WC pellet at 7 s after the beginning of the simulation, just after the peak in the power dissipation curve (a). The cross-section of a real WC pellet after flash sintering (3.7 V and 1000 A) is shown (c) together with FESEM micrographs taken in three areas (red squares) of different density.

flash event, in correspondence of the interfaces between the pellet and the electrodes. The high thermal conductivity of molybdenum (Table 1) is indeed the major contribution to the heat loss from the pellet, generating a strong temperature gradient during the sintering process. To better visualize this gradient and to understand its influence on the densification phenomenon, Fig. 11 compares the simulated temperature reached in the pellet cross-section with the microstructure of a real WC sample obtained by flash sintering. As already discussed in previous works, the densification rate of WC is accelerated during the power surge, when the heating rate is maximum (Fig. 11, a). It is possible to consider that the temperature distribution achieved during the flash event, hence the sintering stage with maximum densification rate, is related to the final density of the material. Fig. 11 (a) and (b) represent exactly the temperature reached within the WC pellet during the power surge, when the heating rate is maximum. The temperature distribution (Fig. 11, b), soon after the power peak, is for sure related to the final microstructure (Fig. 11, c). The top and bottom portions, in contact with the molybdenum electrodes, look darker in the digital image taken on the polished cross-section of a sintered pellet (Fig. 11, c); according to the FESEM analysis, that region possesses a lower density (around 80%). Conversely, the material is almost completely dense (97–98%) in the central part of the pellet, where the highest temperature is achieved. It is also worth comparing the non-homogenous shrinkage of the sintered pellet in the radial direction with the temperature map in Fig. 11 (b). Higher temperatures are reached laterally, due to the insulating zirconia die, and this promotes a greater shrinkage during the densification phenomenon with respect to the radial shrinkage near the top and down sides. This difference results in the peculiar concave lateral shape of the pellet after sintering (Fig. 11,c).

Fig. 11 points out the strict connection between the temperature field, the thermal runaway event and the corresponding densification achieved during an ERFS experiment. The FEM simulation carried out in this work is proven to be a valid tool for studying the flash sintering phenomenon also in non-conventional sintering apparatus, like that presented in Fig. 1. In addition, the agreement between the simulated and the real situation allows one to adopt strategies for improving the flash process. For flash sintering of metallic ceramics, like WC, critical is how the powder is connected to the electrical system. The use of cylindrical metallic electrodes was found to be a great strategy to supply the high current density required for sustaining the flash. On the other side, the use of refractory metals, like Mo, with high thermal conductivity (Table 1), strongly affected the homogeneity of the sintered material in terms of density and microstructure (Fig. 11).

From the present work one can understand the necessity to find new solutions to supply electrical energy to the material, limiting the heat losses through the electrodes during the flash process.

In order to solve this problem one could select a refractory material with very high melting point (2000 °C or above), being at the same time good electronic conductor but bad thermal conductor. This is big challenge from the material science point of view because in metals electrons carry both heat and electrical charge, their electrical and thermal conductivities being therefore coupled as defined by the Wiedemann–Franz law [28,29]. Nevertheless, some peculiar materials violate this law, like VO_2, which shows a separation of the phonons from electronic thermal conductivities. Lee et al. [30] reported an anomalous separation of the heat and charge transport mechanisms in VO_2 near its metal-insulator transition. This material possesses a thermal conductivity of about ~0.2 W/m K and an electrical conductivity of ~8.0×10^5 S/m, this making it a potential candidate to be used as thermal barrier. Since VO_2 electrical conductivity is not as high as metals, being similar to graphite, small cylindrical inserts with a reduced thickness, could be placed between the green sample and the electrodes to reduce the strong heat losses.

4. Conclusions

In the present study a coupled Electromagnetic–Heat transfer finite element model was set-up to predict the flash sintering process of conductive ceramics, like WC. The proposed analysis consistently reproduces the physical phenomenon when compared with experimental data.

At the macroscopic scale, the flash event can be represented as a thermal runaway event driven by the evolution of the material's resistivity when the heat generated exceeds the dissipated one. The present work confirms that a thermal runaway event is also achievable for PTC conductive ceramics if one considers that the material in the green state is initially NTC.

More specifically, it is possible to conclude that.

- A drop of three orders of magnitude in the resistivity, from 10^{-3} to 10^{-6} Ω m, is sufficient to activate a thermal runaway, leading to a burst in the temperature up to more than 1800 °C in a few seconds;
- the localisation of the electric current at the nanometric particle–particle contacts has a prominent role in the onset conditions for the flash event; the overheating at the contact regions of increased electrical resistance allows to initiate the runaway event at lower applied voltage;
- the temperature gradient achieved during the electrical power surge is directly related to the homogeneity of the sintered material; the regions in contact with the electrodes experienced a slower heating and, accordingly, are affected by a higher porosity once the sintering process finishes.

Author contributions

Isacco Mazo: Conceptualization, Methodology, Software, Validation, Formal analysis, Investigation, Data Curation, Writing – Original Draft, Visualization, Project administration. **Barbara Palmieri**: Methodology, Software, Validation, Investigation, Writing – Review & Editing. **Alfonso Martone**: Project administration, Writing – Review & Editing. **Michele Giordano**: Project administration, Writing – Review & Editing. **Vincenzo M. Sglavo**: Writing – Review & Editing, Supervision, Resources, Funding acquisition, Project administration.

Data and code availability

The raw and processed data used to produce this work will be shared by the corresponding author upon reasonable request.

Ethical approval

Not Applicable.

Declaration of Competing Interest

The authors declare that they have no known competing financial interests or personal relationships that could have appeared to influence the work reported in this paper.

Acknowledgments

This work was partially supported within the program Departments of Excellence 2018–2022 (DII-UNITN "E-Mat") – funded by the Italian Ministry of University and Research (MIUR).

REFERENCES

[1] Todd RI, Zapata-Solvas E, Bonilla RS, Sneddon T, Wilshaw PR. Electrical characteristics of flash sintering: thermal runaway of Joule heating. J Eur Ceram Soc 2015;35:1865–77. https://doi.org/10.1016/j.jeurceramsoc.2014.12.022.

[2] Biesuz M, Sglavo VM. Flash sintering of ceramics. J Eur Ceram Soc 2019;39:115–43. https://doi.org/10.1016/j.jeurceramsoc.2018.08.048.

[3] Lagos MA, Agote I, Schubert T, Weissgaerber T, Gallardo JM, Montes JM, et al. Development of electric resistance sintering process for the fabrication of hard metals: processing, microstructure and mechanical properties. Int J Refract Metals Hard Mater 2017;66:88–94. https://doi.org/10.1016/j.ijrmhm.2017.03.005.

[4] Montes JM, Cuevas FG, Ternero F, Astacio R, Caballero ES, Cintas J. Medium-frequency electrical resistance sintering of oxidized C. P. iron powder. Metals (Basel) 2018;8:1–14. https://doi.org/10.3390/met8060426.

[5] Mei Y, Li L, Li X, Li W, Yan H, Xie Y. Electric-current-assisted sintering of nanosilver paste for copper bonding. J Mater Sci Mater Electron 2017;28:9155–66. https://doi.org/10.1007/s10854-017-6649-4.

[6] McWilliams B, Yu J, Kellogg F. Sintering aluminum alloy powder using direct current electric fields at room temperature in seconds. J Mater Sci 2018;53:9297–304. https://doi.org/10.1007/s10853-018-2207-6.

[7] Mazo I, Molinari A, Sglavo VM. Electrical resistance flash sintering of tungsten carbide. Mater Des 2022;213:110330. https://doi.org/10.1016/j.matdes.2021.110330.

[8] Mazo I, Molinari A, Sglavo VM. Effect of pressure on the electrical resistance flash sintering of tungsten carbide. J Eur Ceram Soc 2022;42:2028–38. https://doi.org/10.1016/j.jeurceramsoc.2022.01.017.

[9] Caliman LB, Bichaud E, Soudant P, Gouvea D, Steil MC. A simple flash sintering set-up under applied mechanical stress and controlled atmosphere. MethodsX 2015;2:392–8. https://doi.org/10.1016/j.mex.2015.10.004.

[10] Vikrant KSN, Phuah XL, Lund J, Wang H, Hellberg CS, Bernstein N, et al. Modeling of flash sintering of ionic ceramics. MRS Bull 2021;46:67–75. https://doi.org/10.1557/s43577-020-00012-0.

[11] Yu M, Grasso S, Mckinnon R, Saunders T, Reece MJ. Review of flash sintering: materials, mechanisms and modelling. Adv Appl Ceram 2017;116:24–60. https://doi.org/10.1080/17436753.2016.1251051.

[12] ev Becker MZ, Shomrat N, Tsur Y. Recent advances in mechanism Research and methods for electric-field-assisted sintering of ceramics. Adv Mater 2018;30:1–8. https://doi.org/10.1002/adma.201706369.

[13] Frei W. Control current and voltage sources with the AC/DC module the terminal boundary condition. 2016. https://www.comsol.com/blogs/control-current-and-voltage-sources-with-the-acdc-module/.

[14] Ansori. Sensor technology handbook. Elsevier 2005;3. https://doi.org/10.1016/B978-0-7506-7729-5.X5040-X.

[15] Engineering ToolBox, resistivity and conductivity - temperature coefficients common materials. 2003. https://www.engineeringtoolbox.com/resistivity-conductivity-d_418.html. [Accessed 22 September 2022]. accessed.

[16] Raznjevic K. Handbook of thermodynamic tables. Begell house; 1995.

[17] Alekseev A, Andreenko E, Orlovskiy I, Gorshkov A, Akhtyrsky S, Kozlov A, et al. A study of methods to enhance infrared emissivity of Molybdenum surfaces. Fusion Eng Des 2019;146:144–8. https://doi.org/10.1016/j.fusengdes.2018.12.002.

[18] Schreiber J. Tungsten carbides: structure, properties and application in hardmetals. Springer Series Mater Sci 1990;190. https://doi.org/10.1524/zkri.1990.190.3-4.315.

[19] Pierson HO. Handbook of refractory carbides and nitrides: properties, characteristics, processing and applications. Handbook of Refractory Carbides and Nitrides 1996;100–17. https://doi.org/10.1016/b978-081551392-6.50007-6.

[20] Palmieri B, Cilento F, Siviello C, Bertocchi F, Giordano M, Martone A. Mitigation of heat propagation in a battery pack by interstitial graphite nanoplatelet layer: coupled electrochemical-heat transfer model. Journal of Composites Science 2022;6. https://doi.org/10.3390/jcs6100296.

[21] Ren K, Liu J, Wang Y. Flash sintering of yttria-stabilized zirconia: fundamental understanding and applications. Scripta Mater 2020;187:371–8. https://doi.org/10.1016/j.scriptamat.2020.06.040.

[22] Ren K, Wang Q, Lian Y, Wang Y. Densification kinetics of flash sintered 3mol% Y2O3 stabilized zirconia. J Alloys Compd 2018;747:1073–7. https://doi.org/10.1016/j.jallcom.2018.02.308.

[23] Bram M, Laptev AM, Mishra TP, Nur K, Kindelmann M, Ihrig M, et al. Application of electric current-assisted sintering techniques for the processing of advanced materials. Adv Eng Mater 2020;22. https://doi.org/10.1002/adem.202000051.

[24] Semenov AS, Trapp J, Nöthe M, Eberhardt O, Wallmersperger T, Kieback B. Thermo-electro-mechanical modeling, simulation and experiments of field-assisted sintering. J Mater Sci 2019;54:10764–83. https://doi.org/10.1007/s10853-019-03653-y.

[25] Braunovic M, Konchits Vv, Myshkin NK. Electrical contacts: fundamentals, applications and technology. CRC Press 2017;23. https://doi.org/10.1201/9780849391088.

[26] Chaim R. Numerical model for particle size effects on flash sintering temperature of ionic nanoparticles. J Mater Sci 2018;53:13853–64. https://doi.org/10.1007/s10853-018-2604-x.

[27] Mazo I, Vanzetti LE, Molina-Aldareguia JM, Molinari A, Sglavo VM. Role of surface carbon nanolayer on the activation of flash sintering in tungsten carbide. Int J Refract Metals Hard Mater 2022:106090. https://doi.org/10.1016/j.ijrmhm.2022.106090.
[28] Jonson M, Mahan GD. Mott's formula for the thermopower and the Wiedemann-Franz law. Phys Rev B 1980;21:4223–9. https://doi.org/10.1103/PhysRevB.21.4223.
[29] Yadav A, Deshmukh PC, Roberts K, Jisrawi NM, Valluri SR. An analytic study of the Wiedemann–Franz law and the thermoelectric figure of merit. J Phys Commun 2019;3. https://doi.org/10.1088/2399-6528/ab444a.
[30] Lee S, Hippalgaonkar K, Yang F, Hong J, Ko C, Suh J, et al. Anomalously low electronic thermal conductivity in metallic vanadium dioxide. Science 2021;355(1979):371–4. https://doi.org/10.1126/science.aag0410.